 CMC, vol.27, no.1, pp.55-72, 2012

Identification of Elasto-Plastic Constitutive Parameters by Self-Optimizing Inverse Method: Experimental Verifications

Shen Shang and Gun Jin Yun[1,1]

Abstract: In this paper, the Self-Optimizing Inverse Method (Self-OPTIM) has been experimentally verified by identifying constitutive parameters solely based on prescribed boundary loadings without full-field displacements. Recently the Self-OPTIM methodology was developed as a computational inverse analysis tool that can identify parameters of nonlinear material constitutive models. However, the methodology was demonstrated only by numerically simulated testing with full-field displacement fields and prescribed boundary loadings. The Self-OPTIM is capable of identifying parameters of the chosen class of material constitutive models through minimization of an implicit objective function defined as a function of full-field stress and strain fields in the optimization process. The unique advantages of the Self-OPTIM includes: 1) model independency that is expected to open up a wide range of applications for various engineering simulations; 2) capabilities of parameter identification based solely on global measurements of boundary forces and displacements. In this paper, the Self-OPTIM inverse method is experimentally verified by using two different shapes of specimens made of AISI 1095 steel: 1) dog-bone and 2) notched specimens under a loading and unloading course. Parameters of a cyclic plasticity model with nonlinear kinematic hardening rule and associated flow theory are identified by the Self-OPTIM. Multiple tests and the inverse simulations are conducted to ensure consistent performance of the Self-OPTIM. The identified parameters are successively used to reconstruct the material response.

Keywords: Self-OPTIM, inverse analysis, elasto-plastic constitutive model, parameter indentification.

[1] Corresponding author. Email: gy3@uakron.edu, Tel.: +1-330-972-8489

1 Introduction

As computer and computational technologies are rapidly advanced, complex nonlinear constitutive models have become more and more feasible for use in the design of complex structures. Most constitutive models contain either physical or phenomenological parameters that should be calibrated based on experimental observations. However, as the number of parameters increases, it would be more challenging to determine the parameters from limited availability of laboratory test data. Such difficulties are related to lack of information on the material behavior. Therefore, robust inverse methods for identifying constitutive model parameters are considered of great importance for better predictions of *in-situ* response of materials [Cooreman et al. (2007); Ghaboussi et al. (1998); Ghouati et al. (1998); Grediac et al. (2006a); Pannier et al. (2006); Ponthot et al. (2006)]. In the literature, there are three distinct categories of inverse identification methods: 1) the finite element model updating (FEMU) method [Hild et al. (2006); Mahnken (2000); Pagnacco et al. (2005)]; and 2) the virtual field method (VFM) [Avril et al. (2004); Avril et al. (2008); Grediac et al. (2006b); Grediac et al. (1990); Pierron et al. (2007)]. All of the existing identification methods enforce equilibrium conditions, either in weak or strong form, the constitutive relationships that relate full-field displacements to the stresses, and the boundary conditions. However, they differ in the objective functions they use and in whether they require measured full-field displacements or not.

As updating-based methods, the FEMU methods iteratively update constitutive parameters, minimizing an objective function that represents the error, or gap, between the measured quantity and the corresponding quantity computed by using finite element analyses. The FEMU approach has been applied to model parameter identification for materials with linear elastic [Lecompte et al. (2007)], viscoelastic [Moreau et al. (2006)], elasto-plastic [Kajberg et al. (2004)] and viscoplastic [Kajberg et al. (2007)] behavior. FEMU methods may not require full-field measurements; partial measurements can also be sufficient to determine the constitutive parameters. However, the FEMU methods require iterative finite element analyses, which take a great deal of computational times. In the VFM, a chosen set of kinematically admissible virtual displacement fields is assumed and substituted into the virtual work equation along with full-field displacements measured by the digital image correlation (DIC) technique. This leads to a system of linear equations that can be solved for constitutive parameters [Grediacet al (1990)]. In 2007, Avril and Pierron compared the VFM with FEMU methods based on minimization of a variety of gaps, such as displacement gap, constitutive equation gap, and equilibrium gap. They concluded that FEMU based on "displacement gap" minimization yields equations that are similar to those used by the VFM [Avril et al. (2007)]. The VFM

has an advantage of faster computation times than FEMU approaches; however, it requires full-field measurements obtained by using costly equipment. Moreover, DIC based full-field displacement data are subject to potential measurement errors. The DIC technique has been combined with finite element (FE) simulation to identify key parameters in the material model [Cooreman et al. (2008); M.H.H. Meuwissen (1998)]. The VFM has recently been extended to identify the constitutive parameters that govern elasto-plastic constitutive equations [Grediacet *et al.* (2006a); Pierron *et al.* (2010); Sutton *et al.* (2008)]. On the other hand, Ghaboussi and his co-workers developed an autoprogressive training algorithm that enables artificial neural network (ANN) based material models to be automatically trained through nonlinear finite element analyses under boundary force and displacement measurements from laboratory tests [Ghaboussiet *et al.* (1998)]. The autoprogressive training algorithm is considered an innovative inverse analysis method that can extract local constitutive behavior in ANN forms from the global response observed in the laboratory testing. However, it is limited to the application of ANN based material constitutive models. Inspired by the autoprogressive training algorithm, self-optimization inverse analysis method (Self-OPTIM), a new inverse constitutive parameter identification framework was developed by [Yun et al. (2011)]. In their work, verifications of the Self-OPTIM method was demonstrated for parameter identification of cyclic plasticity model based on numerically simulated tests.

In this paper, the Self-OPTIM is experimentally verified through identification of parameters of an elasto-plasticity constitutive model. The Self-OPTIM methodology has unique advantages: 1) model-independency that opens up a wide range of applications to various engineering simulations; 2) capabilities of parameter identification based solely on global measurements of boundary forces and displacements; and 3) simplicity of implementations with a variety of global optimization tool such as genetic algorithms or gradient-free simplex method. In the Self-OPTIM framework, parameters of a chosen material constitutive model are unknown *a priori*. Two parallel nonlinear finite element simulations are conducted through all load (or time) increment steps per each iterative optimization process by separately imposing two boundary conditions – 1) natural boundary conditions and 2) essential boundary conditions – obtained from the same tested specimen and experimental design on the two finite element models. To this end, an implicit objective function, expressed in terms of full-field stresses and strains from the two nonlinear finite element analyses, is iteratively minimized. This paper is organized as follows: Section 2 briefly describes the chosen material constitutive model, Section 3 presents the Self-OPTIM inverse identification algorithm, Section 4 presents verifications and discussions of the Self-OPTIM method with experimental data, and Section 5 summarizes the conclusions.

2 Material constitutive model

The Self-OPTIM is a model independent inverse identification method in which parameters of any material constitutive model can be identified. Numerous elasto-plastic models are available that can be applied to simulate the inelastic behavior of a material under cyclic loadings. In this paper, a cyclic plasticity model with a non-linear kinematic hardening law (Armstrong–Frederick type), as presented in [Armstrong (1966)] has been adopted. Inaccurate reproductions of experimental results caused by inherent shortcomings of the chosen model should be treated as a modeling error. Thus such limitations of the chosen model should not be considered as defects of the proposed Self-OPTIM methodology.

2.1 Material Constitutive Model

A UMAT material subroutine has been implemented to be used in the Self-OPTIM method. The model is based on the work by Lemaitre and Chaboche [Lemaitre et al. (1990)]. The chosen elasto-plasticity model can reproduce both nonlinear isotropic and kinematic hardening behavior which is commonly observed, but not limited to, in metallic materials.

The associate plastic flow rule under normality hypothesis assumes that the plastic strain increases in a direction normal to the yield surface. However, it is notable that frictional materials such as soils and rock with large dilations or certain metallic alloys used in metal sheet forming violate the associate flow rule. Fundamental assumption in the plasticity theory is the decomposition of the total strain rate into elastic and plastic parts. They are expressed as

$$d\varepsilon = d\varepsilon^e + d\varepsilon^p; \quad d\varepsilon^p_{ij} = d\lambda \frac{\partial f}{\partial S_{ij}} \tag{1}$$

where $d\lambda$ is the plastic multiplier. In the radial return method, trial deviatoric stress increment takes a stress state to outside of the yield surface and then plastic corrector brings back the stress state onto the yield surface in the radial direction. On the π plane, the von Mises yield locus takes a circular form. The multi-axial yield function is expressed as

$$F(\sigma) = \sigma^{tr}_e - r - \sigma_y = 0 \tag{2}$$

$$\sigma^{tr}_e = \sqrt{\frac{3}{2}(\sigma^{tr\_dev}_{ij} - \alpha_{ij})(\sigma^{tr\_dev}_{ij} - \alpha_{ij})} \tag{3}$$

where $\sigma^{tr\_dev}_{ij}$ is the trial deviatoric stress component; α_{ij} is the back stress for nonlinear kinematic hardening; σ_y is the yield stress, and r is the drag stress for

isotropic hardening behavior. The yield function is a nonlinear function of the effective plastic strain. Thus, Newton's iterations should be executed to find the plastic strain increment which is expresses as

$$\Delta\varepsilon^p = \Delta p\mathbf{n} \text{ where } \mathbf{n} = \frac{3}{2}\left(\frac{\sigma^{dev} - \alpha_t}{\sigma_e^{tr}}\right) \tag{4}$$

where $\mathbf{n}$ is the normal direction tensor; Δp is the increment of effective plastic strain; σ^{dev} is the deviatoric stress tensor; α_t is the back stress at the previous converged state time t; and σ_e^{tr} is the effective trial stress.

2.2 Effects of Hardening Parameters on Cyclic Elasto-Plastic Behavior of Materials

For the kinematic hardening behavior, the Amstrong-Frederick type model (A-F model) [Armstrong et al. (1966)] is used for simulating evolutions of the back stress under cyclic loadings. However, it is known that the model has limitations in reproducing ratcheting response of the material and the decomposed nonlinear kinematic hardening models can better predict stresses under cyclic loadings than the conventional A-F model does [Bari et al. (2000)]. As previously mentioned, it is notable that such limitations of the A-F model cannot be claimed as limitations of the proposed Self-OPTIM methodology. To reproduce the Bauschinger effect, the A-F model defines evolutionary equation of the back stress as follows

$$\dot{\alpha}_{ij} = \frac{2}{3}Cn_{ij}\dot{p} - \gamma\alpha_{ij}\dot{p} \tag{5}$$

As the effective plastic strain increment ($\dot{p}$) increases, the rate of the back stress ($\dot{\alpha}_{ij}$) also increases. n_{ij} is a component form of the normal direction tensor ($\mathbf{n}$). Two model parameters C and γ determines the maximum saturated yield stress (C/γ) along the kinematic hardening evolution and γ influences the rate of saturation of the yield stress due to kinematic hardening. Considering such effects of the C and γ parameters on the kinematic hardening and translational evolutions of the yield surface in stress space, at least half-cycle (loading-yielding-unloading-yielding) stress-strain path with a sufficiently large strain range is required to identify the parameters.

A nonlinear isotropic hardening model suggested by Chaboche [Chaboche (1986)] is adopted to simulate expansion of the yield surface under increasing plastic deformations. The rate equation of the isotropic hardening parameter is expressed as

$$\dot{r}(p) = b(Q - r)\dot{p} \tag{6}$$

In Eq. (6), r is the drag stress showing isotropic hardening behavior and Q determines the saturated yield stress $(Q + S_{y0})$ to be reachable during cyclic straining. The value of b determines the rate of the saturation of the yield stress. Eq. (6) is expressed as $r(p) = Q(1 - e^{-bp})$ if integrated with initial value $r = 0$. Thus, depending on the strain range and the parameter b, local stress-strain paths could be sufficient or insufficient for identifying the Q parameter. Under symmetric stress or strain controlled experiments of metallic materials, both isotropic and kinematic hardening effects are combined to generate the cyclic hardening behavior.

Figure 1 illustrates the effect of combined nonlinear isotropic and kinematic hardening on the cyclic hardening response. According to this observation, multiple cycles of stress-strain paths experienced by the material can provide comprehensive information to identify the hardening parameters.

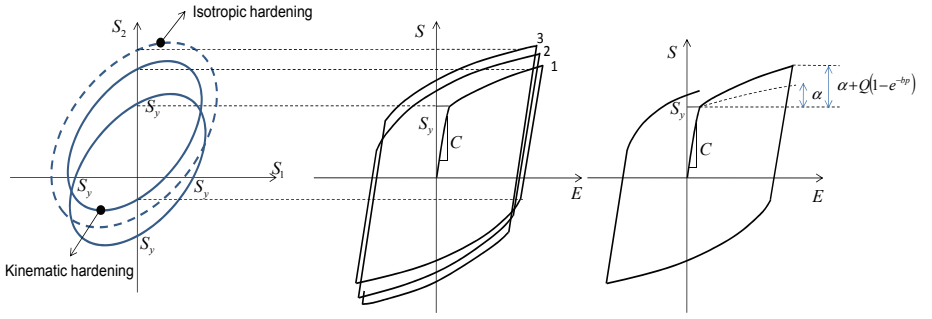

Figure 1: Cyclic Hardening Behavior and Effects of Combined Nonlinear Hardening Model Parameters

As long as sufficient stress-strain data within the linear elastic range are generated, Young's modulus and Poisson ratio could also be identified. Since error of the initial yield stress can create large errors in subsequent stress updates, the yield stress can be identified as long as the material is yielded. However, due to limitations of the testing machine and geometry of specimens used, loading and half of unloading path under tension stress states was used in this paper, for example, in order to avoid buckling during material tests. For those reasons, only nonlinear kinematic hardening was activated in this paper. In the following, the proposed Self-Optimizing inverse method will be introduced with details.

3 Self -Optimization Inverse Analysis Method (Self-OPTIM)

3.1 Capability of the Self-OPTIM Inverse Analysis Method

The Self-OPTIM method was originally developed for parameter identification of material constitutive models based on experimental data such as full-field (or partial field) displacements, global force and displacement boundary loadings. In this paper, further investigation on the Self-OPTIM is conducted to experimentally verify its extensive capability of identifying parameters of material constitutive models using only the global force and displacement boundary loadings measured from laboratory tests. This is considered as an advantageous feature of the Self-OPTIM because the DIC based full-field displacements are always subjected to measurement errors. Unlike the FEMU approaches that directly compare observable responses for experiments and FE simulations, the Self-OPTIM method minimizes an objective function (OF) defined in terms of full-field stresses and strains extracted through a course of two parallel nonlinear finite element simulations along the loading curve. It is notable that stresses and strains are related by constitutive theories.

3.2 Computational Procedures for Self-OPTIM

Figure 2 shows overall computational procedures of the implemented Self-OPTIM method. In the first step, the targeted material is tested under a predefined cyclic loading profile. Potentially it could be any test – such as tension, compression, torsion tests, or more complex multi-axial tests as long as well-defined boundary forces and displacements could be properly measured. It is recommended that loading paths has to be determined based on the parameters to be identified and based on understandings of effects of the parameters on stress predictions. However, identification of optimal loading paths related to experimental design has been addressed in this paper.

Within each optimization iterative step, two nonlinear finite element analyses are conducted using updated material constitutive model parameters under the experimentally measured force and displacement boundary loadings. From the displacement-driven nonlinear FE simulation, stresses (σ_U) and strains (ε_U) are extracted at every Gauss point and load step. Correspondingly, from the force-driven nonlinear FE simulations, stresses (σ_F) and strains (ε_F) are extracted at every Gauss point and load step. The Self-OPTIM method uses an implicit objective function ($OF_{implicit}$, see Eq. (7)) defined as a function of stresses (σ_F, σ_U) and strains (ε_F,

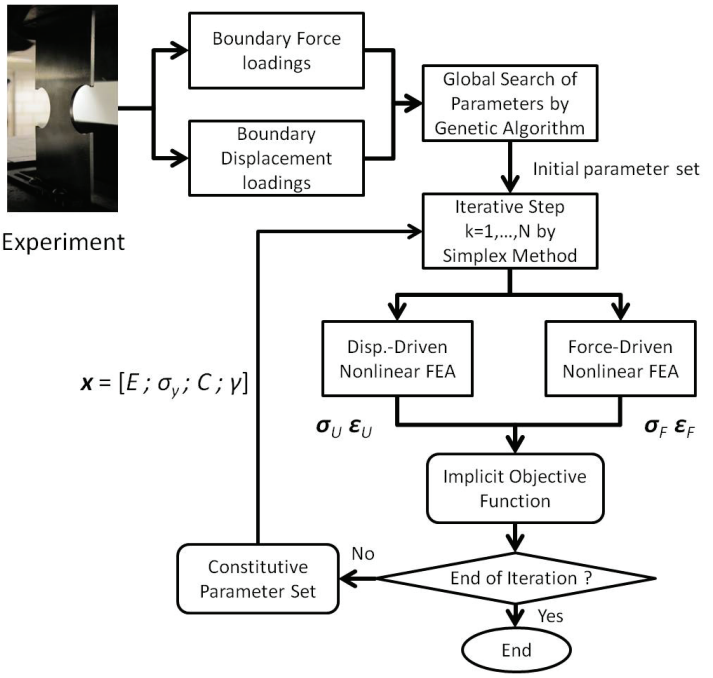

Figure 2: Schematic flowchart of Self-OPTIM inverse analysis method

ε_U),

$$OF_{implicit} = \frac{1}{2}\sum_{k=1}^{LS}\left(1-\frac{\sum_{j=1}^{NE}\sum_{i=1}^{GP}||\sigma_{iU}^{k}||_j}{\sum_{j=1}^{NE}\sum_{i=1}^{GP}||\sigma_{iF}^{k}||_j}\right)^2+\frac{1}{2}\sum_{k=1}^{LS}\left(1-\frac{\sum_{j=1}^{NE}\sum_{i=1}^{GP}||\varepsilon_{iF}^{k}||_j}{\sum_{j=1}^{NE}\sum_{i=1}^{GP}||\varepsilon_{iU}^{k}||_j}\right)^2 \quad (7)$$

where $||\cdot||$ indicates the Euclidean norm; σ_{iF}^{k}, ε_{iF}^{k} and σ_{iU}^{k},ε_{iU}^{k} are the simulated stresses and strains extracted from the zone of interests(ZOI) under force and displacement boundary conditions, respectively; and LS, NE, and GP denote the total number of selected load steps, the total number of selected elements in ZOI, and the total number of Gauss points in the finite elements, respectively.

A fundamental difference between the Self-OPTIM and the other inverse identification methods is that the experimental measurements of displacement, force, and other responses are not used as reference values in the Self-OPTIM. Instead, those experimental measurements act as predefined boundary loadings for the two parallel nonlinear FE simulations. More details on theoretical background and procedures of the Self-OPTIM framework can be found in [Yun *et al.* (2011)].

3.3 Hybrid Genetic-Simplex Algorithm

In this paper, a hybrid genetic-simplex method was employed for efficient searching of the optimum constitutive parameters. The optimization technique used in the Self-OPTIM framework is a combination of genetic algorithm (GA) and simplex methods [Nelder et al. (1965)] (Title: A simplex-method for function minimization). Initially, a total of 200 individuals are randomly generated to form an initial population within feasible bounds. After the $OF_{implicit}$ is evaluated for all individuals, the individual solution giving the minimum $OF_{implicit}$ value is selected as an initial guess for the subsequent simplex method. This procedure first searches for the solution space globally and it is followed by optimization iterations using the simplex method with a reasonable initial input. Therefore, it reduces the possibility of being trapped to a local minimum. The maximum number of iterations is set as a terminating criterion. Therefore, the simplex searching will be terminated when the preset maximum iteration number is reached.

4 Verification of Self-OPTIM Identification with Experiment Test Results

4.1 Material Tests and Predefined Boundary Loading Data

Two types of test specimens – dog-bone specimens (for homogeneous stress tests) and notched specimens (for heterogeneous stress tests) – are used for the purpose of experimentally verifying the Self-OPTIM methodology. Three specimens of each type were cut from the same plate with 2 mm thickness. The geometric dimensions of the specimens and the corresponding finite element models using eight-node plane stress elements are shown in Figure 3. Displacement-controlled uni-axial tension loading and unloading tests were carried out in Y direction by an INSTRON material test machine at a quasi-static strain rate 1.5×10^{-5}. In the homogeneous stress test, three dog-bone specimens were loaded up to a maximum displacement 4.318 mm and unloaded to 4.064 mm. In the heterogeneous stress tests, three notched specimens were loaded up to maximum displacement 2.032 mm and unloaded to 1.778 mm. The displacement and force data were recorded at a sampling frequency of 5 Hz. Data of the full loading path can be divided into three parts: linear elastic, plastic deformation, and linear unloading regions. Due to the measurement noise , the experimental force-displacement data were curve-fitted before they were used in the Self-OPTIM. Approximately, 200 load steps of data (pairs of displacement and force data) were resampled for being imposed to two parallel nonlinear FE simulations used in Self-OPTIM analyses. For applying the boundary forces to the FE model, it is assumed that the boundary force is imposed as uniformly distributed along the gripped line. A group of white-colored elements indicated in Figure 3 was selected as a ZOI from which stresses and strains were

extracted during Self-OPTIM identification processes.

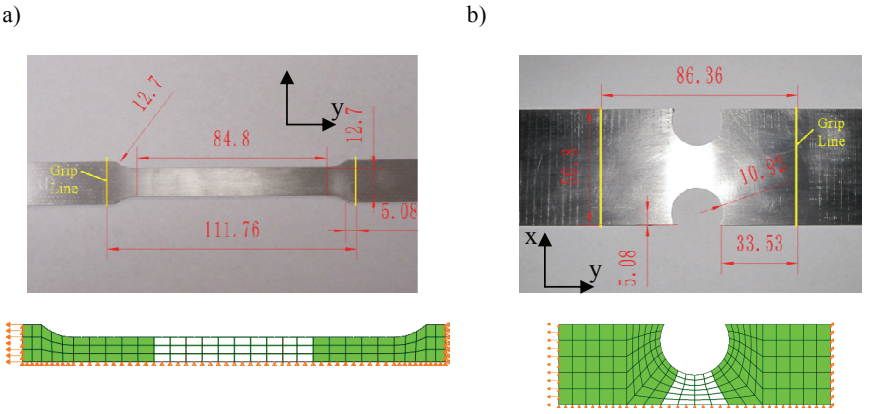

Figure 3: Geometry and FE mesh of the test specimen (all dimensions shown are in mm) (a) dog-bone specimen and (b) notched specimen

It must be noted, however, that data in the plastic regime of the unloading course were not included in the predefined boundary loading because the test data included the geometric softening effect due to buckling under compression in addition to the effect of pure material deformation. According to our numerical studies, inclusions of the unloading hardening curve hindered Self-OPTIM from identifying correct constitutive parameter sets. According to reproduced experimental force-displacement curve by nonlinear FE simulations with the identified parameters, it could be judged that the identified parameters could be very different from the feasible parameters. Therefore, it is important to Self-OPTIM analyses that no geometric softening effect be included in the predefined boundary loading data (i.e. reference data).

4.2 Identification Results and Discussions

A total of six Self-OPTIM inverse analyses were conducted to identify the constitutive model parameters: three for dog-bone shape specimens and three for notched specimens. Good convergence was observed in all of the Self-OPTIM inverse analyses. Identification results of the unknown parameter set are summarized in Table 1 and Table 2. The mean value and the standard error ($=\sigma/n^{1/2}$ where σ is the standard deviation and n is the number of samples) of each identified parameter are plotted in Figure 4.

It can be observed that the identified parameters have good agreement with each

Table 1: Identification results from Self-OPTIM of dog-bone specimen

	Dog-bone Specimen				
	1	2	3	Mean	Standard error
E (GPa)	92.582	95.430	97.450	95.154	1.412
σ_y(MPa)	276.604	295.633	268.254	280.164	8.102
C (GPa)	6.618	5.528	6.197	6.114	0.317
γ	51.251	45.591	48.801	48.548	1.638

Table 2: Identification results of from Self-OPTIM of notched specimen

	Notched Specimen				
	1	2	3	Mean	Standard error
E (GPa)	88.804	87.625	97.471	91.300	3.104
σ_y(MPa)	305.052	291.531	272.329	289.637	9.494
C (GPa)	4.188	5.146	6.573	5.302	0.693
γ	29.661	34.243	37.112	3.672	2.170

other in both specimen types. The six force-displacement curves were reconstructed by using nonlinear FE simulations in which the model parameters identified by Self-OPTIM were used. When compared with the corresponding curves from experimental tests, all of them were observed to be identical. Verification results of the first notched specimen are shown in Figure 5. Therefore it was demonstrated that the Self-OPTIM is able to identify the parameter set that can represent the experimental data accurately.

To further examine the identification results, two simulations were conducted for cross comparisons in which the mean values of the parameters identified from dog-bone shape specimens were used to predict the force-displacement response of notched specimens and vice versa. Because the specimens are made of the same material, the force-displacement curves are expected to be identical in an ideal case. However, slight discrepancy between the reconstructed curves observed in Figure 6(a) and Figure 6(b) is attributable to the stochastic process associated with materials. First, considering the stochastic process in detail, it must be noted that the material has inherited variability; in reality, every material point has different material properties. Secondly, the material pre-hardening caused by manufacturing process could be different between the dog-bone and notched specimens; this could lead to different yield stresses and hardening behavior in the two specimen types. Finally, the modeling error caused by gripping is inevitable in each test; it is challenging to exactly align the grip position in the lab to that of the finite element

model.

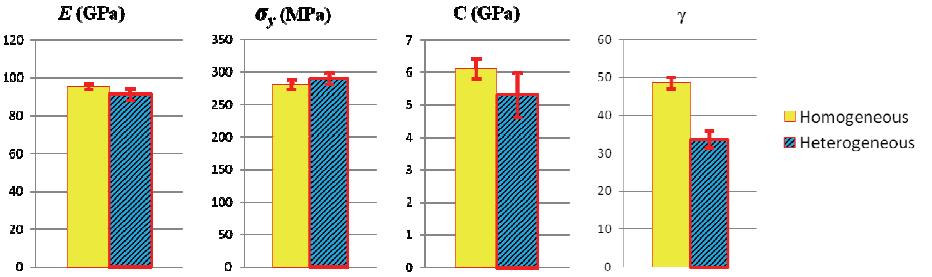

Figure 4: Mean value and standard error of the identified parameters in homogenous and heterogeneous test

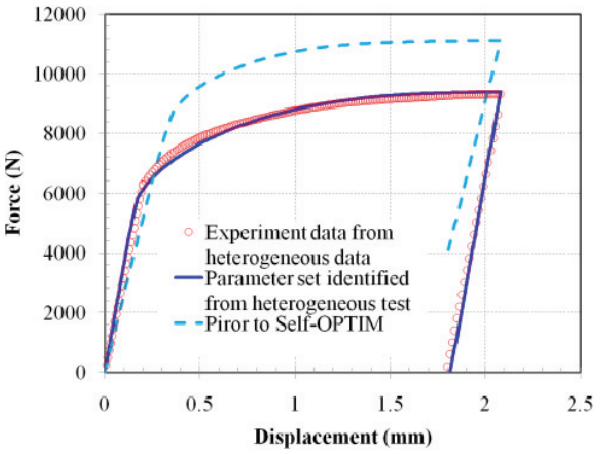

Figure 5: Comparison of the force-displacement curves reconstructed by using the parameters prior to Self-OPTIM, after Self-OPTIM and experiment data

In order to show progress of self-calibration by the Self-OPTIM analysis, the stress and strain distribution from force-driven and displacement-driven simulations by using initial parameter set and identified parameter set at a certain load step are shown in Figure 7. It is observed that correlation of stresses and strains between two parallel simulations significantly increase after Self-OPTIM simulations.

Normalized longitudinal stresses and strains extracted from force-driven and displacement-driven simulations of the notched specimen were plotted at different stages

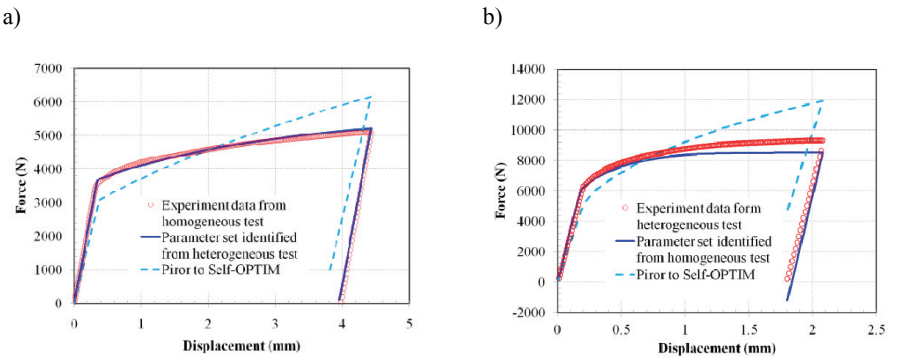

Figure 6: a) Reconstructed force-displacement curve of the dog-bone specimen by the parameter set identified by notched specimens; b) reconstructed force-displacement curve of the notched specimen by the parameter set identified from dog-bone specimens

of Self-OPTIM analyses as shown in Figure 8. First, a parameter set prior to Self-OPTIM was used in the simulations. As shown in the first column of Figure 8, the stresses and strains simulated under two boundary loading conditions were very different. After five iterations of Self-OPTIM, the two sets of stresses and strains have better agreements. Finally, the two sets of stresses and strains become almost identical since the parameter set is well identified after the Self-OPTIM analyses. The correlation coefficient (R), root mean squared error (RMSE), and mean absolute error (MAE) of stresses and strains between force-driven and displacement-driven simulations at different iterative steps are calculated by Eq. (8) to Eq. (10). The statistical indices are defined as follows

$$R = \frac{\sum_n \left(A_n - \bar{A}\right)\left(B_n - \bar{B}\right)}{\sqrt{\left(\sum_n \left(A_n - \bar{A}\right)^2\right)\left(\sum_n \left(B_n - \bar{B}\right)^2\right)}} \tag{8}$$

$$RMSE = \sqrt{\frac{\sum_n (A_n - B_n)^2}{n}} \tag{9}$$

$$MAE = \frac{\sum_n |A_n - B_n|}{n} \tag{10}$$

Where A_n and B_n are two vectors to be compared. The results are listed in Table 3. As the optimization iteration proceeds, it was observed that R value approaches to

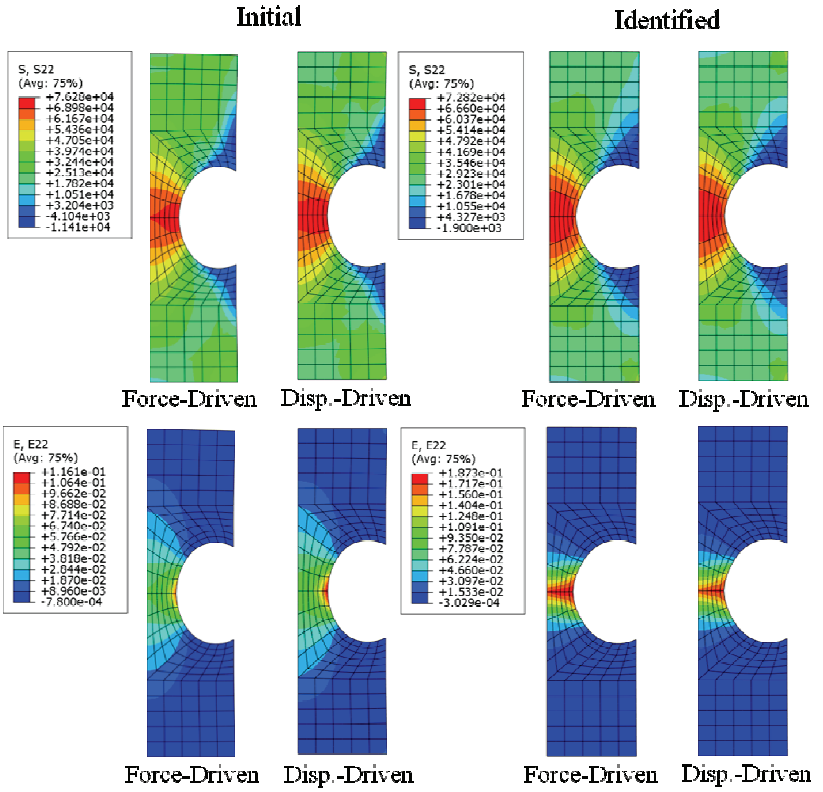

Figure 7: Stress and Strain distributions of the notched specimen on longitudinal direction at 150th load step are compared between force-driven and displacement-driven analyses by using initial parameter set and identified parameter set

one, and both RMSE and MAE values decrease significantly.

Table 3: Statistic analysis of stresses and strains of a notched specimen from force-driven and displacement-driven simulations

	R		**RMSE**		**MAE**	
	σ	ε	σ	ε	σ	ε
Prior to Self-OPTIM	0.83618	0.89493	0.13622	0.14433	0.11511	0.12003
5th Iteration	0.99775	0.93077	0.01530	0.11163	0.01172	0.09385
After Self-OPTIM	0.99882	0.99892	0.01281	0.01122	0.01005	0.00704

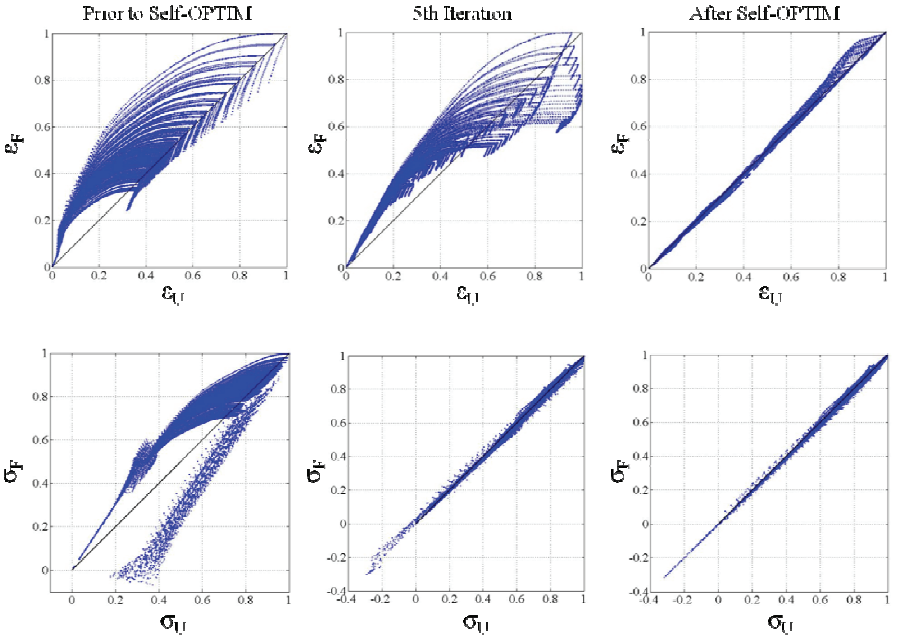

Figure 8: Plots of normalized longitudinal stresses and strains of a notched specimen from force-driven and displacement-driven simulations using the parameter set prior to Self-OPTIM, at the 5th optimization iteration, and after Self-OPTIM

5 Conclusions

In this paper, a novel inverse parameter identification methodology, Self-OPTIM, was verified experimentally. Unlike other existing inverse identification methods, the verified Self-OPTIM method does not need any full-field displacement data. By using only the global force and displacement boundary loadings that can readily be measured from experimental tests, parameters of the elasto-plastic model were successfully identified. Two different geometric types of specimen were used with intentions for verification of generality of the identified parameters. For statistical analysis of test results, three specimens were tested for each geometric type. Parameters identified through the Self-OPTIM were evaluated for reproducing global and local material response. The Self-OPTIM analysis provided consistent parameter sets, and it was proven that the identified parameters could predict *in-situ* material response. While Young's modulus and yield stress were very consistent for multiple tests and different geometries of the specimens, two hardening parameters showed relatively larger difference between dog-bone shape specimens and

notched specimens. It is considered that this difference is a result of the stochastic process associated with materials and the insensitivity of the parameters to stresses and strains.

Acknowledgement: This research is supported by the New Faculty Startup Fund from the University of Akron. The authors are grateful for this support.

References

Armstrong, P.J.; Frederick, C.O., (1966): A Mathematical Representation of the Multiaxial Bauschinger Effect. Berkeley Nuclear Laboratories.

Armstrong, P.J., Frederick, C.O., (1966): A Mathematical Representation of the Multiaxial Bauschinger Effect.

Avril, S.; Grediac, M.; Pierron, F., (2004): Sensitivity of the virtual fields method to noisy data. *Computational Mechanics* 34, 439-452.

Avril, S.; Huntley, J.M.; Pierron, F.; Steele, D.D., (2008): 3D heterogeneous stiffness reconstruction using MRI and the virtual fields method. *Experimental Mechanics* 48, 479-494.

Avril, S.; Pierron, F., (2007): General framework for the identification of constitutive parameters from full-field measurements in linear elasticity. *International Journal of Solids and Structures* 44, 4978-5002.

Bari, S.; Hassan, T., (2000): Anatomy of coupled constitutive models for ratcheting simulation. *International Journal of Plasticity* 16, 381-409.

Chaboche, J.L., (1986): Time-Independent Constitutive Theories for Cyclic Plasticity. *International Journal of Plasticity* 2, 149-188.

Cooreman, S.; Lecompte, D.; Sol, H.; Vantomme, J.; Debruyne, D., (2007): Elasto-plastic material parameter identification by inverse methods: Calculation of the sensitivity matrix. *International Journal of Solids and Structures* 44, 4329-4341.

Cooreman, S.; Lecompte, D.; Sol, H.; Vantomme, J.; Debruyne, D., (2008): Identification of mechanical material behavior through inverse modeling and DIC. *Experimental Mechanics* 48, 421-433.

Ghaboussi, J.; Pecknold, D.A.; Zhang, M.F.; Haj-Ali, R.M., (1998): Autoprogressive training of neural network constitutive models. *International Journal for Numerical Methods in Engineering* 42, 105-126.

Ghouati, O.; Gelin, J.C., (1998): Gradient based methods, genetic algorithms and the finite element method for the identification of material parameters. *Simulation of Materials Processing: Theory, Methods and Applications*, 157-162

993.

Grediac, M.; Pierron, F., (2006a): Applying the virtual fields method to the identification of elasto-plastic constitutive parameters. *International Journal of Plasticity* 22, 602-627.

Grediac, M.; Pierron, F.; Avril, S.; Toussaint, E., (2006b): The virtual fields method for extracting constitutive parameters from full-field measurements: A review. *Strain* 42, 233-253.

Grediac, M.; Vautrin, A., (1990): A New Method for Determination of Bending Rigidities of Thin Anisotropic Plates. *Journal of Applied Mechanics-Transactions of the Asme* 57, 964-968.

Hild, F.; Roux, S., (2006): Digital image correlation: from displacement measurement to identification of elastic properties - a review. *Strain* 42, 69-80.

Kajberg, J.; Lindkvist, G., (2004): Characterization of materials subjected to large strains by inverse modelling based on in-plane displacement fields. *International Journal of Solids and Structures* 41, 3439-3459.

Kajberg, J.; Wikman, B., (2007): Viscoplastic parameter estimation by high strain-rate experiments and inverse modeling - Speckle measurements and high-speed photography. *International Journal of Solids and Structures* 44, 145-164.

Lecompte, D.; Smits, A.; Sol, H.; Vantomme, J.; Van Hemelrijck, D., (2007): Mixed numerical-experimental technique for orthotropic parameter identification using biaxial tensile tests on cruciform specimens. *International Journal of Solids and Structures* 44, 1643-1656.

Lemaitre, J.; Chaboche, J.L., 1990. Mechanics of Solid Materials. Cambridge University Press.

M.H.H. Meuwissen, C.W.J.o., F.P.T. Baaijiens, R. Petterson, J.D. Janssen, (1998): Determination of the elasto-plastic properties of aluminium using a mixed numerical-experimental method. *Journal of Materials Processing Technology* 75, 204-211.

Mahnken, R., (2000): A comprehensive study of a multiplicative elastoplasticity model coupled to damage including parameter identification. *Computers & Structures* 74, 179-200.

Moreau, A.; Pagnacco, E.; Borza, D.; Lemosse, D., 2006. An evaluation of different mixed experimental/numerical procedures using FRF for the identification of viscoelastic materials, International conference on noise and vibration engineering ISMA, Leuven.

Nelder, J.A.; Mead, R., (1965): A Simplex-Method for Function Minimization. *Computer Journal* 7, 308-313.

Pagnacco, E.; Lemosse, D.; Hild, F.; Amiot, F., 2005. Inverse strategy from

displacement field measurement and distributed forces using FEA, SEM Annual Conference and Exposition on Experimental and Applied Mechanics, Poland.

Pannier, Y.; Avril, S.; Rotinat, R.; Pierron, F., (2006): Identification of elasto-plastic constitutive parameters from statically undetermined tests using the virtual fields method. *Experimental Mechanics* 46, 735-755.

Pierron, F.; Avril, S.; Tran, V.T., (2010): Extension of the virtual fields method to elasto-plastic material identification with cyclic loads and kinematic hardening. *International Journal of Solids and Structures* 47, 2993-3010.

Pierron, F.; Vert, G.; Burguete, R.; Avril, S.; Rotinat, R.; Wisnom, M.R., (2007): Identification of the orthotropic elastic stiffnesses of composites with the virtual fields method: Sensitivity study and experimental validation. *Strain* 43, 250-259.

Ponthot, J.P.; Kleinermann, J.P., (2006): A cascade optimization methodology for automatic parameter identification and shape/process optimization in metal forming simulation. *Computer Methods in Applied Mechanics and Engineering* 195, 5472-5508.

Sutton, M.A.; Yan, J.H.; Avril, S.; Pierron, F.; Adeeb, S.M., (2008): Identification of heterogeneous constitutive parameters in a welded specimen: Uniform stress and virtual fields methods for material property estimation. *Experimental Mechanics* 48, 451-464.

Yun, G.J.; Shang, S., (2011): A Self-Optimizing Inverse Analysis Method for Estimation of Cyclic Elasto-Plasticity Model Parameters. *International Journal of Plasticity* 27, 576-595.